

CERN-TH/95-143  
 GEF-TH-5/1995  
 IFUM 506/FT  
 hep-ph/yymmxxx

DIFFERENTIAL DISTRIBUTIONS FOR  
 HEAVY FLAVOUR PRODUCTION AT HERA

**Stefano Frixione<sup>1</sup>**

Dip. di Fisica, Università di Genova, Genoa, Italy

**Paolo Nason<sup>2</sup>**

CERN TH-Division, CH-1211 Geneva 23, Switzerland

**Giovanni Ridolfi**

INFN, Sezione di Genova, Genoa, Italy.

**Abstract**

We compute pseudorapidity and transverse momentum distributions for charm and bottom production at HERA. We examine the effect of next-to-leading order QCD corrections, the effect of possible intrinsic transverse momenta of the incoming partons, and of fragmentation. We compare our results with those of a full Monte Carlo simulation using HERWIG. The importance of the hadronic component of the photon is also studied. We examine the possibility of distinguishing between different parametrizations of the photon parton densities using charm production data, and the possibility of extracting information about the small- $x$  behaviour of the gluon density of the proton. We also give a prediction for the transverse momentum and pseudorapidity distributions for bottom production at HERA.

CERN-TH/95-143/95

May 1995

---

<sup>1</sup>Address after June 1: ETH, Zurich, Switzerland

<sup>2</sup>On leave of absence from INFN, Sezione di Milano, Milan, Italy.

## 1. Introduction

Experimental results on charm photoproduction at HERA have recently become available [1]. It is likely that more detailed results on the differential distributions will appear in the near future. With respect to previous photoproduction experiments (ref. [2]) HERA offers the new opportunity of a higher energy regime. A theoretical study of the total photoproduction cross section has already been given in ref. [3]. In the present work we extend the analysis of ref. [3] (to which we refer the reader for a general introduction and for notation) by considering single inclusive distributions for heavy flavour production at HERA. Our analysis is based on the next-to-leading order calculation of heavy-quark photoproduction and hadroproduction cross sections performed in refs. [4,5], as implemented in a computer program developed in refs. [6,7]. We will consider cross sections at fixed photon energies. When necessary, a discussion of the energy dependence of the distributions will be given. We will also consider electroproduction for small photon virtuality, in the Weizsäcker-Williams approximation, which is appropriate for the bulk of the photoproduction cross section. We will not consider the production of heavy flavours in deeply inelastic events, i.e. events in which high photon virtuality is required (see refs. [8]). The paper is organized as follows. In section 2 we study the point-like contribution of the transverse momentum and pseudorapidity distributions in photoproduction. Section 3 is devoted to the study of the hadronic component, considering the possibility of separating it from the point-like component with appropriate cuts. In sections 4 and 5 we consider electroproduction of charm and bottom, in the Weizsäcker-Williams approximation. In section 6 we compare our fixed-order results with those of the Monte Carlo HERWIG [9], and in section 7 we give our conclusions. Some technical details on the factorization schemes, the scale dependence, and the modified Weizsäcker-Williams approximation used here are given in the Appendix.

## 2. point-like component

Unless specifically stated, we will use in the following the set of parton densities MRSA, ref. [10], with  $\Lambda_5 = 151$  MeV. This set of distribution functions has been recently updated (MRSG, ref. [11]), to include new HERA deep inelastic scattering data, allowing a different small- $x$  behaviour of the gluon and sea quark densities. We have checked that the shapes of the single-inclusive distributions we are considering

are not significantly different when the new parametrization is used. The default value of the charm quark mass will be  $m_c = 1.5$  GeV. The renormalization scale will be taken as  $\mu_R = \mu_0$ , and the factorization scale for the proton and for the photon will be taken as  $\mu_F = \mu_\gamma = 2\mu_0$ , where  $\mu_0 = \sqrt{p_T^2 + m_c^2}$ . We begin by showing the transverse momentum distribution for the charm quark in fig. 1, for  $E_\gamma = 25$  GeV (the proton energy  $E_p$  will be fixed in the following to be 820 GeV). We also show

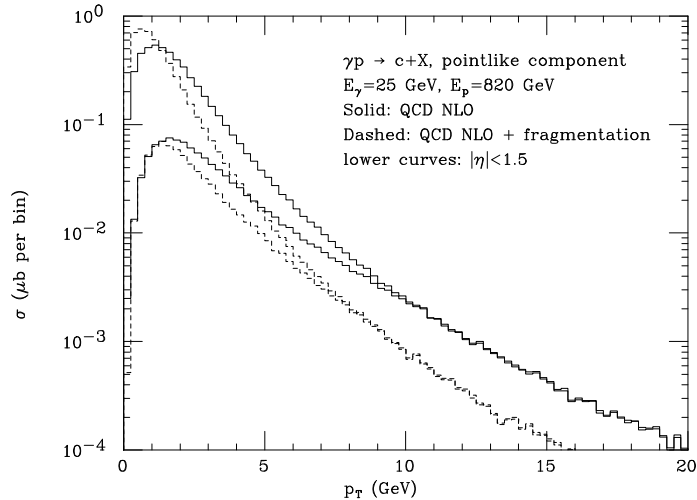


Figure 1: *Charm transverse momentum distribution in photon-proton collisions, with and without a pseudorapidity cut. The effect of applying a Peterson fragmentation function to the final-state quark is also shown.*

the effect of applying the Peterson fragmentation function [12]

$$D(x) = \frac{1}{x(1 - 1/x - \epsilon/(1-x))^2} \quad (2.1)$$

to the final state quark. We use the value  $\epsilon = 0.06$ , which is the central value quoted in ref. [13] for charm quarks. As can be expected this softens considerably the  $p_T$  spectrum. As discussed in ref. [14], in the case of fixed target photoproduction experiments, the inclusion of Peterson fragmentation correctly reproduces the shape of the measured  $p_T$  distribution. The effect of a pseudorapidity cut similar to the one applied by the ZEUS collaboration [1] is also shown. At low to moderate  $p_T$  this cut considerably lowers the cross section, while at higher  $p_T$  it has a negligible effect. In fig. 2 we compare the  $p_T$  distributions at different photon energies. We also illustrate

the effect of applying an intrinsic transverse momentum  $k_T$  to the incoming parton (see ref. [14]). We find that even with the very large value of  $\langle k_T^2 \rangle = 2 \text{ GeV}^2$  the effect is small. Therefore, in the following, we will neglect the effect of an intrinsic transverse momentum of the incoming partons.

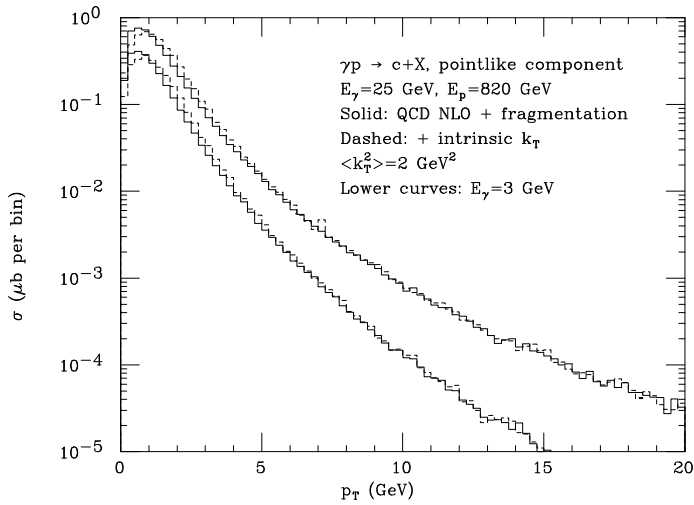


Figure 2: *Charm transverse momentum distribution in photon-proton collisions, for two values of the photon energy. The effect of applying an intrinsic transverse momentum to the incoming parton is also shown.*

Pseudorapidity distributions for charm are shown in fig. 3 for  $E_\gamma = 25 \text{ GeV}$ . We observe that the point-like contribution to the cross section at this energy strongly favours large negative pseudorapidities. A cut on the transverse momentum of the produced quark tends to move the distribution towards the central region. The dotted curve shows the effect of fragmentation in the presence of a transverse momentum cut. The fragmentation has little effect on the pseudorapidity of the quark, but degrades its transverse momentum, so that the  $p_T$  cut has a stronger effect. The effect of fragmentation without transverse momentum cut is not shown in the figure, since it is not well defined (see ref. [14]). At lower energies (fig. 4) the pseudorapidity distributions become more central.

We now turn to the sensitivity of our distributions to the various parameters that enter the computation. We have studied the dependence of our distributions upon the charm quark mass, by varying it between 1.2 and 1.8 GeV, on the renormalization

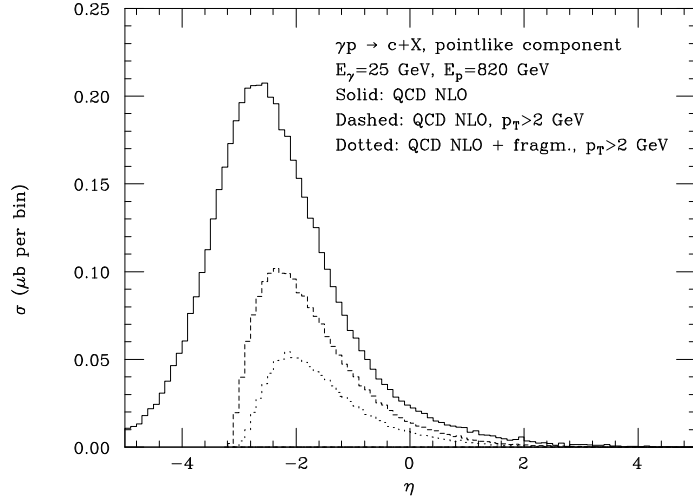


Figure 3: *Charm pseudorapidity distribution in photon-proton collisions, with and without a transverse momentum cut. The effect of fragmentation is also shown.*

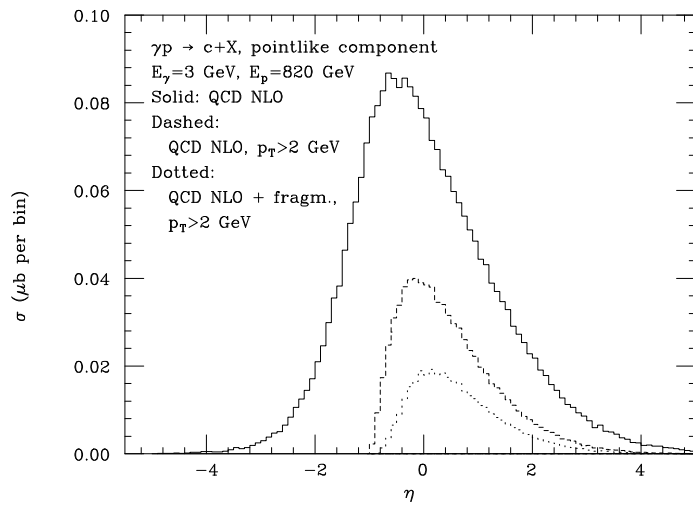


Figure 4: *As in fig. 3, for  $E_\gamma = 3$  GeV.*

scale, which was varied by a factor of 2 below and above its default value, and upon the distribution functions, by considering the MRSD–' [15] and the CTEQ2MF [16] sets. The proton parton densities were chosen in order to span the allowed range for the small- $x$  behaviour of the gluon density, MRSD–' being the most singular, and CTEQ2MF the least singular one (see ref. [3] for a discussion of this point). Studying the variation of our results with respect to  $\Lambda$  is a difficult problem, since the values of  $\Lambda$  extracted from fits to deep inelastic scattering data are not in good agreement with the LEP value. The CTEQ group has provided a parton density set in which the value of  $\Lambda$  was pushed as high as possible (see also ref. [17]). They use a value of  $\Lambda_5 = 220$  MeV, which is still below the LEP value, but adequate for a study of the sensitivity of the distributions. The set of parton densities obtained in this fit (CTEQ2ML) was used in association with this value of  $\Lambda$ .

We found that the only cases in which there is a noticeable shape variation is in the  $p_T$  distributions when we vary the mass and the parton densities. The relevant plots are given in figs. 5 and 6. From the figures we can see a comparable variation of the

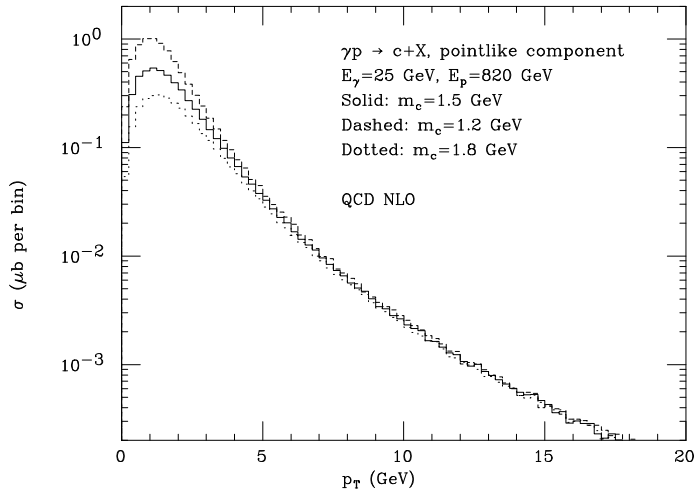


Figure 5: *Mass dependence of the  $p_T$  distribution of charm.*

$p_T$  spectrum in the low momentum region in the two cases. The mass dependence is easily understood. We expect nearly no mass dependence at high transverse momenta, while in the massless limit the cross section diverges at small momenta. Therefore, the smaller the mass, the higher the cross section at low  $p_T$ . As far as the distribution function dependence is concerned, the small- $x$  uncertainty in the densities plays here

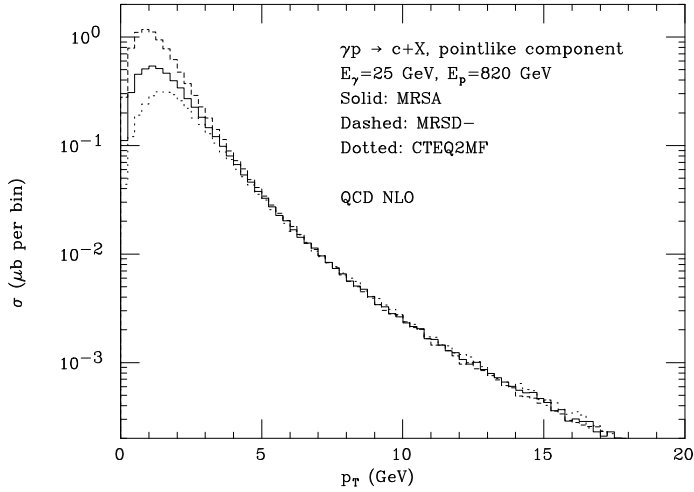


Figure 6: *Sensitivity of the  $p_T$  distribution of charm to the parton densities.*

a major rôle. The more singular the small- $x$  behaviour, the higher the cross section at small  $p_T$ .

As a last point, we observe that, when measuring the total cross section, if a transverse momentum cut on the  $p_T$  spectrum is being applied, the extrapolated total cross section will depend upon the assumptions we make about the value of the mass and the small- $x$  behaviour of the distribution functions. This has to be properly taken into account when inferring properties of the parton density at small  $x$  from the energy behaviour of the total charm cross section.

### 3. Hadronic component

The point-like contribution of the charm cross sections will be contaminated by the hadronic component. Depending upon the chosen distribution functions for the photon, the contribution of the hadronic component to the total cross section may dominate over the point-like one. Whatever the choice of the distribution functions, however, the two components differ remarkably in the pseudorapidity distribution. The point-like component, as we have seen, favours negative pseudorapidities, while the hadronic component favours the positive direction. The separation of the two components will therefore require an analysis of a large pseudorapidity range. In the

following, we will show a study of the full (i.e. point-like plus hadronic) pseudorapidity distribution for different choices of photon and proton distribution functions. We will see that the shape and magnitude of the  $\eta$  distribution will allow us to distinguish between the most extreme parametrizations of photon distribution functions. In fig. 7 we show the  $\eta$  distribution, obtained with the LAC1 [18] set of photon parton densities, and three different sets of proton parton densities; both the point-like and the full results are presented. A similar plot for the GRV [19] set for the photon is

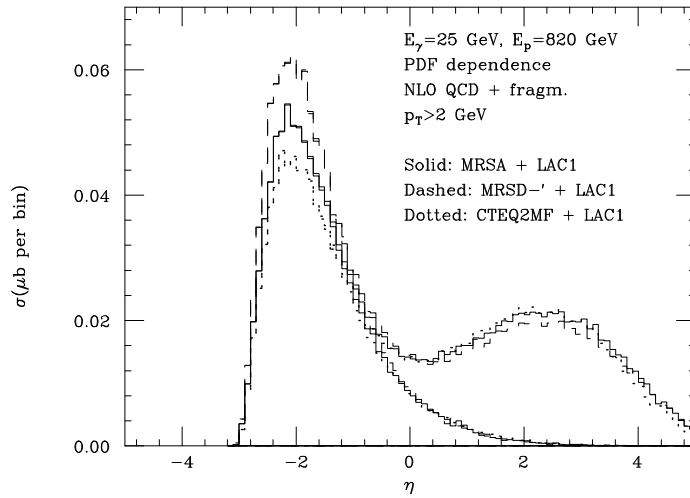


Figure 7: *Pseudorapidity distribution of charm quarks, obtained with the LAC1 set of photon parton densities, and three different sets of proton parton densities. The point-like component is also shown.*

given in fig. 8. We have chosen the LAC1 and GRV sets because, for our purposes, they represent the two extreme possibilities, as discussed in ref. [3]. In figs. 7 and 8 we have imposed a realistic transverse momentum cut, which in general will make the pseudorapidity distribution even narrower. In spite of the cut, the separation of the two contributions is quite apparent.

The study of the pseudorapidity distribution could help in distinguishing among different proton parton density sets, especially if the large negative pseudorapidity region could be explored. On the other hand, the large difference in shape induced by the two photon sets considered has measurable effects even in the central region.

The full transverse momentum distribution is presented in fig. 9. The point-like and hadronic contributions are also separately shown. From the figure, we can see

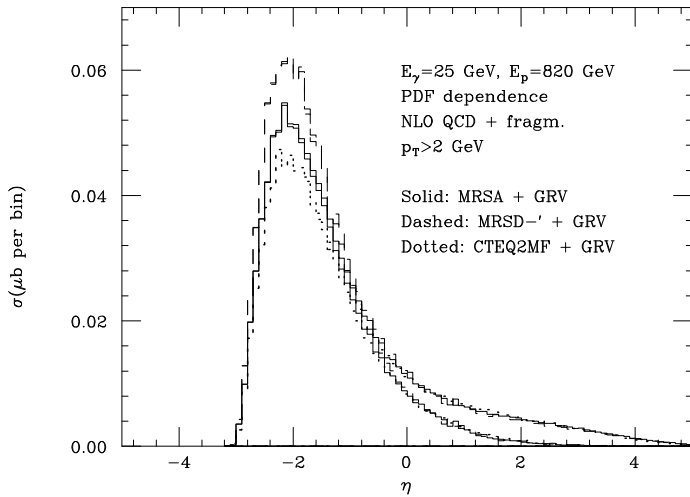


Figure 8: *Pseudorapidity distribution of charm quarks, obtained with the GRV set of photon parton densities, and three different sets of proton parton densities. The point-like component is also shown.*

that the hadronic contribution is dominant in the low- $p_T$  region. At  $p_T \simeq 2$  GeV, it amounts to 50% of the full cross section. Therefore, even without investigating the very low- $p_T$  region, the softer behaviour of the full cross section with respect to the point-like one should be visible. Obviously, this behaviour is strongly influenced by the photon parton densities used. If the GRV set were used, instead of the LAC1 set, the full distribution would differ only slightly from the point-like one already at moderate  $p_T$ . We can conclude that the charm transverse momentum spectrum at large values of the photon energy could help in further constraining the parton densities in the photon. From fig. 7, we also learn that asymmetric pseudorapidity cuts may enhance or suppress the effect of the hadronic component in the  $p_T$  spectrum, thus providing another handle for its study.

#### 4. Charm electroproduction

In this section we discuss single-inclusive distributions for charm production in electron-proton collisions in the Weizsäcker-Williams approximation. We take the electron and proton energies to be 27.5 GeV and 820 GeV, respectively. Since the Weizsäcker-Williams function peaks in the small- $x$  region, the bulk of the contribution

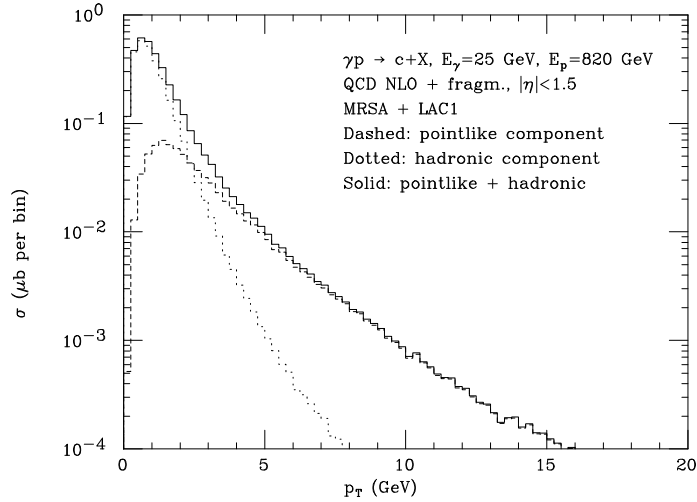


Figure 9: *Transverse momentum distribution of charm quarks. The pointlike and hadronic contributions are separately shown, together with the sum of the two.*

to the cross section will be due to photons of relatively low energy. Therefore, the rôle of the hadronic component is less important with respect to the monochromatic photon case. By applying a small- $p_T$  cut, the contribution of the hadronic component is even more suppressed, especially for soft photon parton densities. Therefore, the QCD predictions at next-to-leading order are less affected by the uncertainty originating from the photon distribution functions.

Because of the softness of the incoming photons, the pseudorapidity distribution of the point-like component is concentrated in the central region. This can be seen in fig. 10, where we show the pseudorapidity distribution for charm quarks, supplemented with Peterson fragmentation and a transverse momentum cut. The hadronic component is computed using our two extreme sets of photon parton densities. It is apparent that its effect is small in the central pseudorapidity region explored at HERA. The curves in fig. 10 are obtained with  $m_c = 1.5$  GeV,  $\mu_R = \mu_0$ ,  $\mu_F = \mu_\gamma = 2\mu_0$  and the MRSA set for proton parton densities. While the total cross section is quite sensitive to the value of these parameters, as shown in ref. [3], the shape of the single-inclusive distributions is rather stable. The pseudorapidity distribution shape is only mildly dependent upon the choice of proton parton densities. This is due to the fact that the various parametrizations differ in the small- $x$  region, which is not deeply

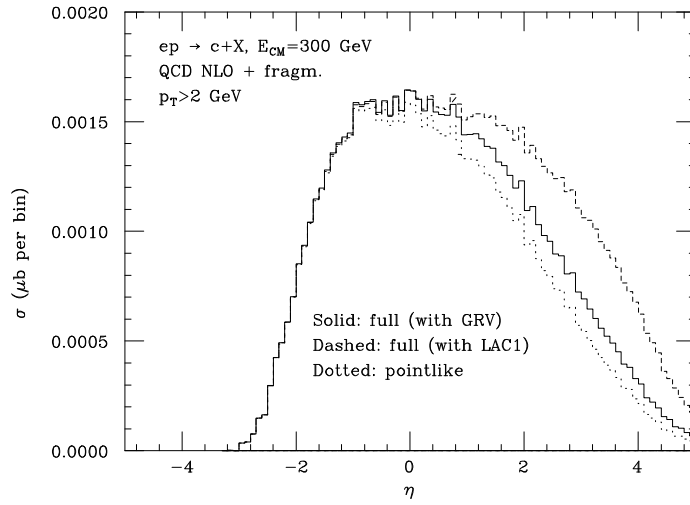


Figure 10: *Pseudorapidity distribution for charm electroproduction. The proton parton density set MRSA is used.*

probed in the electroproduction process. This is shown, for the point-like component, in fig. 11. The proton parton density dependence of the hadronic component is completely negligible, due to the softness of the partons in the electron.

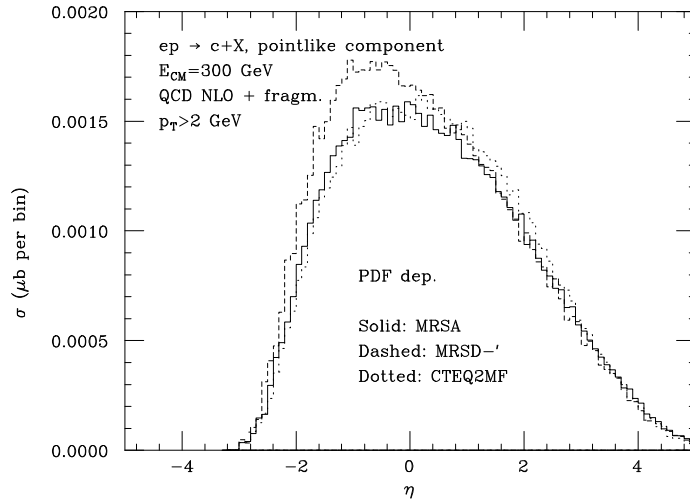


Figure 11: *Proton parton density dependence of the pseudorapidity distribution for charm electroproduction; only the point-like component is shown.*

We now consider the transverse momentum distribution. In fig. 12 we show the point-like contribution to this differential cross section, with and without Peterson fragmentation. The softening of the distribution due to fragmentation should be observable at HERA. The effect of applying a pseudorapidity cut is also shown: it affects the shape of the distribution less dramatically than in the case discussed in section 2. We have checked that the hadronic component contribution to this

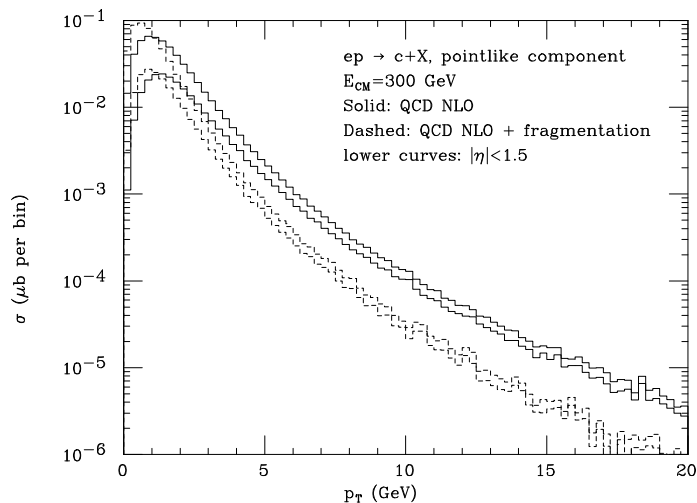


Figure 12: *Transverse momentum distribution for charm electroproduction (point-like contribution).*

distribution is remarkably softer than the point-like one. In practice, its effect is less than 10% for  $p_T > 2$  GeV when fragmentation is included and the pseudorapidity cut  $|\eta| < 1.5$  is applied. We have also computed the same distribution for different values of the renormalization and factorization scales, and we found that the corresponding shape variations are small.

All the distributions presented so far were also evaluated in the case when an antitag condition on the outgoing electron is applied, that is to say when the electron scattering angle is below a given value, which we chose to be 5 mrad. For this computation, the improved form of the Weizsäcker-Williams distribution presented in ref. [20] is appropriate (see the appendix). Differences in the shapes of the distributions are found to be small. As an example, we show in fig. 13 the pseudorapidity distribution with and without the antitag condition described above. The antitag condition has the effect of decreasing the total cross section, as described in ref. [3],

of slightly enhancing the contribution of positive pseudorapidities, and of mildly softening the transverse momentum spectrum.

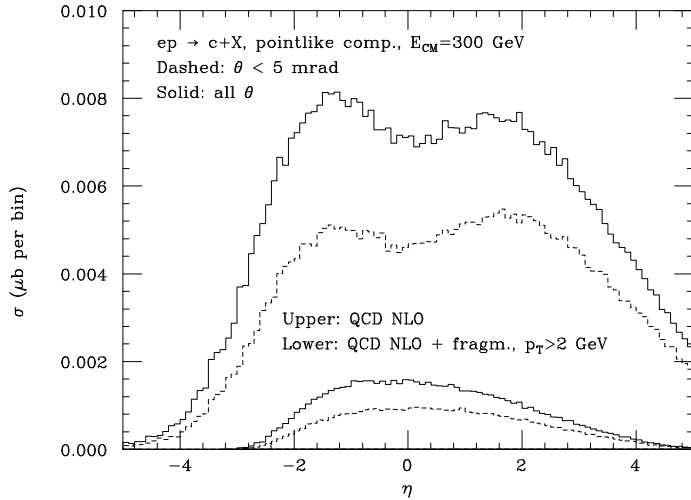


Figure 13: *Pseudorapidity distribution for charm electroproduction, with and without an antitag condition on the scattered electron.*

We can conclude that charm electroproduction distributions are rather insensitive to the choice of the parameters entering the perturbative calculation. Therefore, single-inclusive charm electroproduction will be of little help in constraining the parton distribution functions of both the proton and the photon. On the other hand, the comparison between data and theoretical predictions will be useful for the study of the production mechanism.

## 5. Bottom electroproduction

Due to the higher value of the quark mass, perturbative QCD predictions for bottom production are more reliable than those for charm. Furthermore, we are able to study the scale dependence in an exhaustive manner. In fact, the factorization scale, when varied by a factor of two below and above its default value, is always higher than the minimum allowed by the distribution function parametrizations. In fig. 14 we show the point-like component of the pseudorapidity distribution for bottom electroproduction. The solid curve represents our central prediction, which corresponds

to choosing  $m_b = 4.75$  GeV,  $\mu_R = \mu_F = \mu_\gamma = \mu_0$ , where  $\mu_0 = \sqrt{p_T^2 + m_b^2}$ . The QCD result is supplemented with Peterson fragmentation with  $\epsilon = 0.006$ , the central value of ref. [13] for bottom quarks. In the case of bottom the effect of fragmentation is less important than in the case of charm. The band between the two dashed curves has been obtained by varying the bottom quark mass between 4.5 and 5 GeV and the renormalization and factorization scales between  $\mu_0/2$  and  $2\mu_0$ . The proton parton density set chosen is MRSA. We also show (dotted curve) the result obtained with a parton density set fitted at a higher value of  $\Lambda_{QCD}$ , namely the set CTEQ2ML with  $\Lambda_5 = 220$  MeV, and the central values of mass and scales. It is difficult to foresee

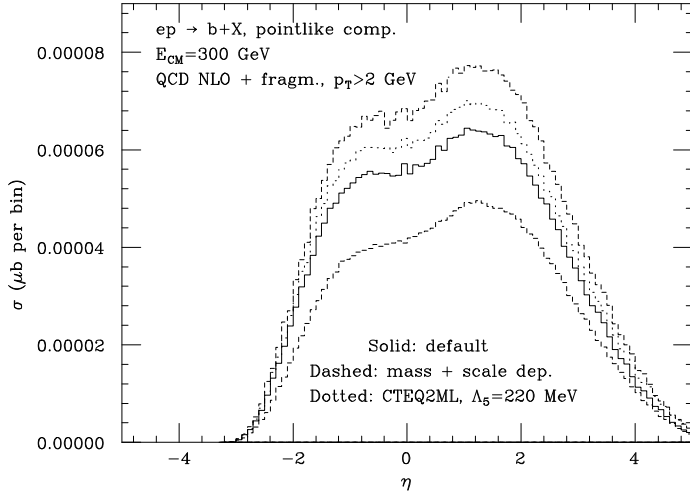


Figure 14: *Pseudorapidity distribution for bottom electroproduction (pointlike component only), with Peterson fragmentation and a transverse momentum cut.*

what a realistic transverse momentum cut could be for bottom production, and we have therefore kept the same cut  $p_T > 2$  GeV we used in the charm case.

Figure 14 does not describe the uncertainties on the theoretical prediction completely, because the CTEQ2ML set was used keeping the scales and the mass at their default value, and because the hadronic contribution was not included. The full uncertainty on the  $\eta$  distribution is presented in fig. 15, in which mass and scales are varied also when using the CTEQ2ML set, and the possibility is considered that the effect of the hadronic component is as large as the LAC1 set implies, or is completely absent. The dramatic effect of the inclusion of the hadronic component is apparent

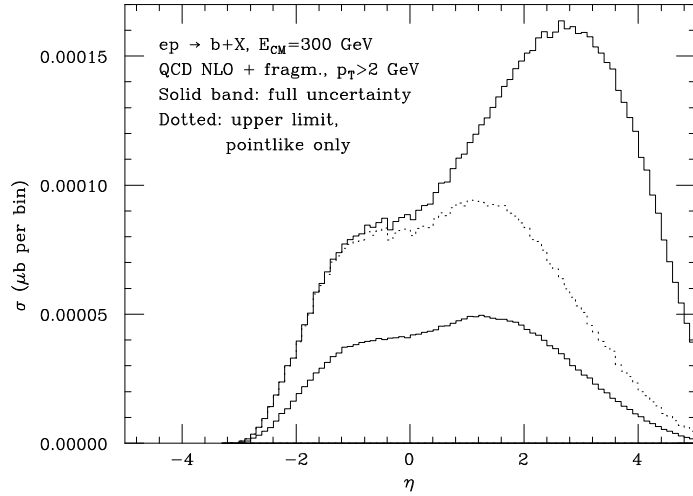


Figure 15: *Full uncertainty on the pseudorapidity distribution for bottom electroproduction with Peterson fragmentation and a transverse momentum cut.*

in the positive pseudorapidity region. This is due to the very soft behaviour of the LAC1 partons and to the stronger sensitivity of the hadronic component to the choice of mass and scales with respect to the one of the point-like component.

We now turn to the transverse momentum distribution, shown in fig. 16, which is analogous to the corresponding figure for the  $\eta$  distribution, fig. 14. As expected, in the large- $p_T$  region the sensitivity to mass and scales choice is strongly reduced. Therefore, the perturbative prediction becomes more reliable there.

The full uncertainty on the  $p_T$  distribution is given in fig. 17, which is analogous to fig. 15. From the figure, it is quite clear that even with the LAC1 set the hadronic component affects the prediction only marginally. This fact is a consequence of the applied pseudorapidity cut, as can be inferred from fig. 15. We can therefore regard fig. 17 as a reliable prediction of QCD for the  $p_T$  spectrum of  $b$  hadrons at HERA.

## 6. Comparison with Monte Carlo results

In order to assess the influence of higher-order and non-perturbative contributions on the shape of single-inclusive distributions, we have compared our fixed-order

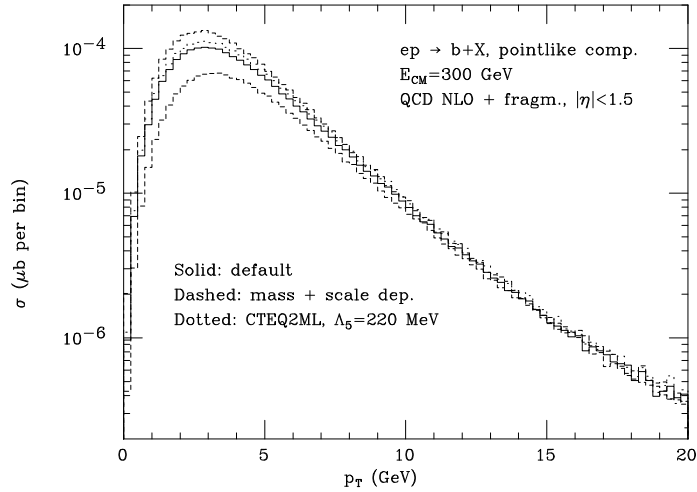


Figure 16: *Transverse momentum distribution for bottom electroproduction (point-like component only) with Peterson fragmentation and a pseudorapidity cut.*

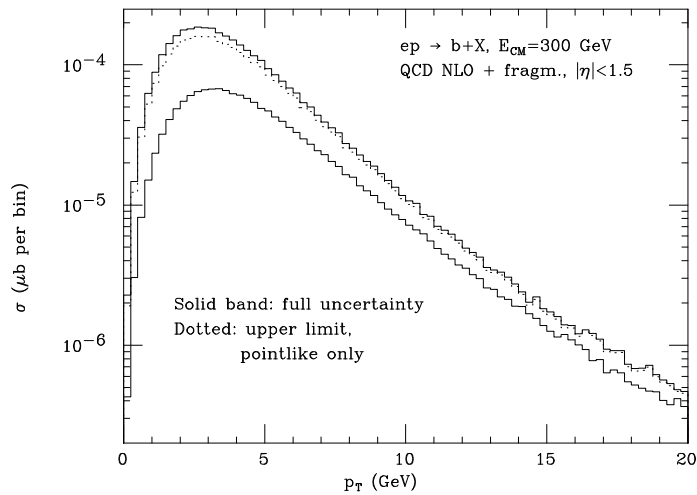


Figure 17: *Full uncertainty on the transverse momentum distribution for bottom electroproduction with Peterson fragmentation and a transverse momentum cut.*

calculations with the results obtained with the parton-shower Monte Carlo program HERWIG [9]. When using HERWIG we have always excluded the flavour excitation processes. This is because comparable processes, such as gluon splitting, are difficult to include. We have therefore preferred to use the Monte Carlo at a consistent level of accuracy. As discussed in section 2, the effect of an intrinsic transverse momentum of the incoming partons is negligible in photoproduction at HERA energies. This leads us to expect that higher-order and non-perturbative corrections are not as important here as in the case of hadroproduction [14]. On the other hand, it is interesting to investigate how Peterson fragmentation compares with the model of cluster hadronization implemented in HERWIG. We limit our discussion to the point-like component of the photoproduction cross section for fixed photon energy.

In fig. 18 we show the transverse momentum distribution computed in fixed-order perturbation theory and with HERWIG. All HERWIG curves have been normalized to give the same total cross section of the corresponding next-to-leading order QCD predictions. We observe that before the hadronization process is switched on, the

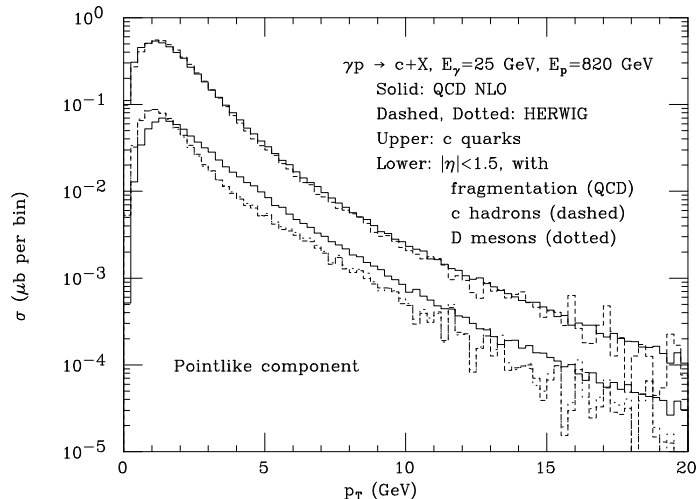


Figure 18: *Transverse momentum distribution for charm photoproduction (point-like component) as given by next-to-leading order QCD and by the Monte Carlo HERWIG.*

QCD prediction and the HERWIG result agree almost perfectly in all the presented  $p_T$  range (upper curves). We then consider the effect of hadronization in the central pseudorapidity region ( $|\eta| < 1.5$ ) by comparing the perturbative prediction supple-

mented with Peterson fragmentation and the HERWIG results for charmed hadrons or  $D$  mesons only (lower curves). In this case the two predictions display a different behaviour only in the low- $p_T$  region. This is also the only part of the  $p_T$  spectrum that is significantly affected by the pseudorapidity cut. The results in fig. 18 allow us to conclude that Peterson fragmentation gives a description of the hadronization process, which is consistent with the one suggested by cluster models only at sufficiently large transverse momenta.

A similar study for the pseudorapidity distribution is presented in fig. 19. In this

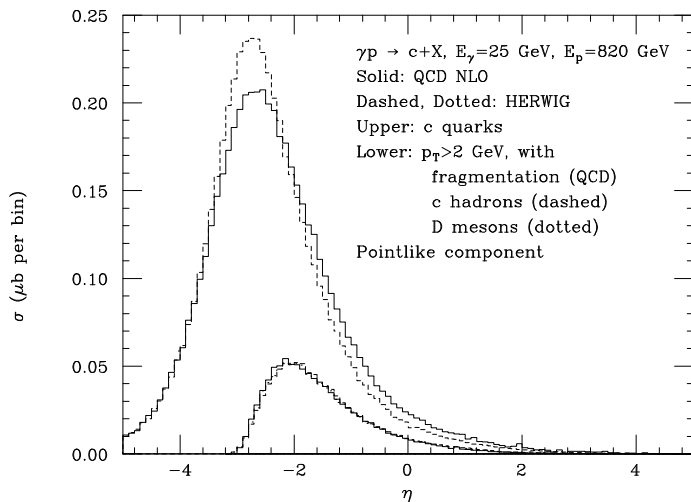


Figure 19: *Pseudorapidity distribution for charm photoproduction (point-like component) as given by next-to-leading order QCD and by the Monte Carlo HERWIG.*

case, some difference is observed between the two distributions before hadronization, the fixed-order QCD prediction being slightly broader. However, they are peaked around the same value of  $\eta$ , which is rather far from the central region, where the experimental acceptance is larger. Applying a small transverse momentum cut, the use of Peterson fragmentation becomes possible also for the pseudorapidity distribution. We are therefore able to compare the QCD next-to-leading order distribution, convoluted with the Peterson fragmentation function, and the HERWIG curves for charmed hadrons. We find a complete agreement between the two.

We have performed the same kind of analysis on the hadronic component, and we found that the qualitative behaviour is completely analogous to what has been

presented for the point-like component.

## 7. Conclusions

We have studied single-inclusive cross sections for charm and bottom production at HERA. We considered charm production in monochromatic photon-proton collisions, for energies spanning the range accessible at HERA. We found that the shape of the  $p_T$  and pseudorapidity distributions are quite stable with respect to the variation of the input parameters entering the calculation. On the other hand, the total cross section value (see ref. [3] for a discussion on this point) is strongly affected by the choice of parameters. We found that from the study of the pseudorapidity distributions in the central  $\eta$  region ( $|\eta| < 1.5$ ) it is difficult to distinguish between the various proton parton densities with different small- $x$  behaviour. On the other hand, the striking difference between the predictions obtained by using the LAC1 and GRV set for photon distribution functions is clearly visible. This fact is almost completely due to the very soft behaviour of the LAC1 parton densities.

The transverse momentum distribution for large  $p_T$  is reliably predicted by QCD. Measurements in this region should constitute a good test of the production mechanism. At moderate  $p_T$ , the point-like result is strongly influenced by the hadronic contribution when the LAC1 set for photon parton densities is used. Experimental investigations in this region of the spectrum could therefore help to distinguish among the various parton distribution functions in the photon.

Charm electroproduction is a less clean test of the production mechanism with respect to monochromatic photon production, because of the convolution with the Weizsäcker-Williams function. On the other hand, the softness of the latter implies a strongly reduced dependence of the total cross section upon the phenomenological parameters entering the calculation. Furthermore, when a small transverse momentum cut is applied, the hadronic contribution is more suppressed than the point-like one, whatever the photon densities used. Therefore, electroproduction is less sensitive to the contamination of the hadronic component than photoproduction with a monochromatic photon, and can be used to further investigate the point-like production mechanism. Unfortunately, a sizeable dependence upon charm mass and renormalization scale remains in the total cross section prediction.

The case in which an antitag condition is applied on the outgoing electron was

also studied. Aside from the effect on the total cross section value (which has already been discussed in ref. [3]), the angular cut slightly enhances the importance of the central pseudorapidity region and mildly softens the transverse momentum spectrum.

We also considered the production of bottom quarks in  $ep$  collisions. Due to the higher value of the quark mass, perturbative QCD predictions for bottom production are more reliable than those for charm. It turns out that the point-like component is quite stable in shape. The hadronic component has a dramatic effect on the pseudorapidity distribution, although less important than in the case of charm. Its effect in the central  $\eta$  region is however marginal. We are therefore able to give a reliable prediction of the  $p_T$  spectrum for  $b$  hadrons in the central  $\eta$  region.

Finally, we compared our results with those obtained using the parton shower Monte Carlo HERWIG. We limited our discussion to the point-like component for monochromatic photon-proton collisions. As far as open charm quark is concerned, we found perfect agreement for the  $p_T$  distribution, in the whole range considered. The next-to-leading order QCD prediction for pseudorapidity distribution is instead slightly broader than the one given by HERWIG in the region around the peak. This difference is however immaterial in the central pseudorapidity region, which is explored by the experiments. We also point out that, without any small transverse momentum cut, differential cross sections in “longitudinal” quantities such as  $\eta$  are indeed not characterized by a true hard scale. In this case, differences between perturbative QCD and parton shower approach are expected. Coming to charmed hadron production, we compared HERWIG prediction with QCD calculation supplemented with the Peterson fragmentation function. A small- $p_T$  cut was applied. The agreement is surprisingly good in the whole  $\eta$  range, while the two predictions for transverse momentum distribution differ in shape only in the small- $p_T$  region.

## Acknowledgements

We wish to thank G. Iacobucci, M. Mangano, J. Roldan, M. Seymour and B. Webber for useful discussions.

## Subtraction schemes in photoproduction

A differential photoproduction cross section can be written as

$$d\sigma^{(\gamma H)}(P_\gamma, P_H) = d\sigma_{\text{point}}^{(\gamma H)}(P_\gamma, P_H) + d\sigma_{\text{hadr}}^{(\gamma H)}(P_\gamma, P_H), \quad (.1)$$

where the quantities in the right-hand side of this equation are the so-called point-like (or direct) and hadronic (or resolved) photon cross sections. In QCD [21],

$$\begin{aligned} d\sigma_{\text{point}}^{(\gamma H)}(P_\gamma, P_H) &= \sum_j \int dx f_j^{(H)}(x, \mu_F) d\hat{\sigma}_{\gamma j}(x P_H, \alpha_s(\mu_R), \mu_R, \mu_F, \mu_\gamma) \quad (.2) \\ d\sigma_{\text{hadr}}^{(\gamma H)}(P_\gamma, P_H) &= \sum_{ij} \int dx dy f_i^{(\gamma)}(x, \mu_\gamma) f_j^{(H)}(y, \mu_F) d\hat{\sigma}_{ij}(x P_\gamma, y P_H, \alpha_s(\mu_R), \mu_R, \mu_F, \mu_\gamma). \quad (.3) \end{aligned}$$

In the case of heavy quark production at next-to-leading order, the short distance partonic cross sections are given by

$$\begin{aligned} d\hat{\sigma}_{\gamma j}(p_1, p_2, \alpha_s(\mu_R), \mu_R, \mu_F, \mu_\gamma) &= \alpha_{\text{em}} \alpha_s(\mu_R) d\sigma_{\gamma j}^{(0)}(p_1, p_2) \\ &\quad + \alpha_{\text{em}} \alpha_s^2(\mu_R) d\hat{\sigma}_{\gamma j}^{(1)}(p_1, p_2, \mu_R, \mu_F, \mu_\gamma) \quad (.4) \end{aligned}$$

$$\begin{aligned} d\hat{\sigma}_{ij}(p_1, p_2, \alpha_s(\mu_R), \mu_R, \mu_F, \mu_\gamma) &= \alpha_s^2(\mu_R) d\sigma_{ij}^{(0)}(p_1, p_2) \\ &\quad + \alpha_s^3(\mu_R) d\hat{\sigma}_{ij}^{(1)}(p_1, p_2, \mu_R, \mu_F, \mu_\gamma). \quad (.5) \end{aligned}$$

In dimensional regularization, we have

$$\begin{aligned} d\hat{\sigma}_{\gamma j}^{(1)}(p_1, p_2) &= d\sigma_{\gamma j}^{(1)}(p_1, p_2, \frac{1}{\epsilon}) + \frac{1}{2\pi} \sum_k \int dx \left( \frac{1}{\epsilon} P_{k\gamma}(x) - H_{k\gamma}(x) \right) d\sigma_{kj}^{(0)}(xp_1, p_2) \\ &\quad + \frac{1}{2\pi} \sum_k \int dx \left( \frac{1}{\epsilon} P_{kj}(x) - K_{kj}^{(H)}(x) \right) d\sigma_{\gamma k}^{(0)}(p_1, xp_2); \quad (.6) \end{aligned}$$

$$\begin{aligned} d\hat{\sigma}_{ij}^{(1)}(p_1, p_2) &= d\sigma_{ij}^{(1)}(p_1, p_2, \frac{1}{\epsilon}) + \frac{1}{2\pi} \sum_k \int dx \left( \frac{1}{\epsilon} P_{ki}(x) - K_{ki}^{(\gamma)}(x) \right) d\sigma_{kj}^{(0)}(xp_1, p_2) \\ &\quad + \frac{1}{2\pi} \sum_k \int dx \left( \frac{1}{\epsilon} P_{kj}(x) - K_{kj}^{(H)}(x) \right) d\sigma_{ik}^{(0)}(p_1, xp_2), \quad (.7) \end{aligned}$$

where  $d\sigma_{\gamma j}^{(1)}$  ( $d\sigma_{\gamma j}^{(0)}$ ) and  $d\sigma_{ij}^{(1)}$  ( $d\sigma_{ij}^{(0)}$ ) are the full,  $d$ -dimensional regulated partonic cross sections at the next-to-leading (leading) order for the point-like and hadronic

contributions respectively. The  $1/\epsilon$  singularities in  $d\sigma_{ij}^{(1)}$  and  $d\sigma_{\gamma j}^{(1)}$  are appropriately subtracted on the right-hand side of eqs. (6), (7).

The  $P_{ij}$  are the usual Altarelli-Parisi splitting function;  $P_{j\gamma}$  is the kernel for the splitting process  $\gamma \rightarrow j + \bar{j}$ , which is equal to  $P_{qg}$  up to a colour factor. The functions  $K_{ij}^{(H)}$ ,  $K_{ij}^{(\gamma)}$  and  $H_{k\gamma}$  are completely arbitrary, in that they define an extra finite part of the subtraction; different choices correspond to different subtraction schemes. In eqs. (6) and (7) the  $\overline{\text{MS}}$  scheme is equivalent to  $H = K = 0$ . For greater generality, we have admitted the possibility to have different subtraction schemes on photon and hadron legs. A change in the subtraction scheme implies that parton distribution functions are modified as follows

$$f'_i = f_i + \frac{\alpha_{\text{em}}}{2\pi} H_i + \frac{\alpha_s}{2\pi} \sum_j K_{ij} \otimes f_j. \quad (8)$$

The term  $H$  is present only in the photon case, and it is a direct consequence of the inhomogeneous term in the modified Altarelli-Parisi equations. In ref. [22] a factorization scheme ( $\text{DIS}_\gamma$ ) for the photon densities is introduced, which uses  $K = 0$  and  $H \neq 0$ . As can be seen for eqs. (6) and (7), the  $\text{DIS}_\gamma$  scheme is therefore equivalent to  $\overline{\text{MS}}$  as far as the hadronic component is concerned. It does however modify the point-like component through the second term in the right-hand side of eq. (6), which is also responsible for a subtraction on the photon leg. This clearly shows that the point-like and the hadronic component are closely related, and that they should not be considered separately. In principle, when considering the variation with respect to  $\mu_\gamma$ , cancellations occur between the hadronic and the point-like components, resulting in renormalization group invariance of the physical cross section  $d\sigma^{(\gamma H)}$  up to terms of order  $\alpha_{\text{em}}\alpha_s^3$ .

Photoproduction cross sections are usually linked to electroproduction ones by a convolution with the Weizsäcker-Williams function [23]:

$$d\sigma^{(eH)}(P_e, P_H) = \int dx f(x, \mu_{WW}) d\sigma^{(\gamma H)}(x P_e, P_H). \quad (9)$$

At HERA, the H1 and ZEUS experiments can directly investigate the virtuality of the exchanged photon, by tagging the emitted electron and retaining only those events in which the electron scattering angle  $\theta$  satisfies the condition  $\theta < \theta_c$ , with  $\theta_c$  typically of the order of few mrad. In ref. [20] a functional form especially suited for this experimental set-up was proposed, namely

$$f(x, E_e) = \frac{\alpha_{\text{em}}}{2\pi} \left\{ 2(1-x) \left[ \frac{m_e^2 x}{E_e^2 (1-x)^2 \theta_c^2 + m_e^2 x^2} - \frac{1}{x} \right] \right\}$$

$$+ \frac{1 + (1 - x)^2}{x} \log \frac{E_e^2 (1 - x)^2 \theta_c^2 + m_e^2 x^2}{m_e^2 x^2} \Big\}, \quad (10)$$

where  $E_e$  is the incoming electron energy in the laboratory frame. When no angular cut is applied, eq. (9) is too restrictive; we relax it by writing

$$d\sigma^{(eH)}(P_e, P_H) = \int dx f(x, \mu_{WW}) d\sigma_{point}^{(\gamma H)}(x P_e, P_H) + \int dx f(x, \mu'_{WW}) d\sigma_{hadr}^{(\gamma H)}(x P_e, P_H), \quad (11)$$

with  $\mu_{WW} \neq \mu'_{WW}$  (for a discussion of the  $\mu_{WW}$  and  $\mu'_{WW}$  values, see ref. [3] and references therein). Strictly speaking, the fact that  $\mu_{WW} \neq \mu'_{WW}$  gives up the renormalization group invariance of the physical cross section in eq. (11), in that no cancellation occurs between the point-like and the hadronic component when variation with respect to  $\mu_\gamma$  is considered. In practice, we have verified that this effect is numerically negligible, the point-like component being almost invariant with respect to  $\mu_\gamma$  variations.

## References

- [1] M. Derrick *et al.*, ZEUS Coll., preprint DESY-95-013, 1995.
- [2] P. Frabetti *et al.*, E687 Coll., *Phys. Lett.* **B308**(1993)193;  
J. C. Anjos *et al.*, E691 Coll., *Phys. Rev. Lett.* **62**(1989)513;  
M. P. Alvarez *et al.*, NA14/2 Coll., *Z. Phys.* **C60**(1993)53;  
G. Bellini, Proceedings of “Les Rencontres de Physique de la Vallée d’Aoste”,  
La Thuile, Aosta Valley, 6-12 March, 1994.
- [3] S. Frixione, M.L. Mangano, P. Nason and G. Ridolfi, *Phys. Lett.* **B348**(1995)633.
- [4] R.K. Ellis and P. Nason, *Nucl. Phys.* **B312**(1989)551.
- [5] P. Nason, S. Dawson and R.K. Ellis, *Nucl. Phys.* **B303**(1988)607; **B327**(1988)49.
- [6] M.L. Mangano, P. Nason and G. Ridolfi, *Nucl. Phys.* **B373**(1992)295.
- [7] S. Frixione, M.L. Mangano, P. Nason and G. Ridolfi, *Nucl. Phys.* **B412**(1994)225.
- [8] E. Laenen, S. Riemersma, J. Smith and W.L. van Neerven,  
*Nucl. Phys.* **B392**(1993)162;  
S. Riemersma, J. Smith and W.L. van Neerven, *Phys. Lett.* **B347**(1995)143;  
B.W. Harris and J. Smith, preprint ITP-SB-95-08, hep-ph/9503484.
- [9] G. Marchesini, B.R. Webber, G. Abbiendi, I. G. Knowles,  
M. H. Seymour and L. Stanco, *Comp. Phys. Comm.* **67**(1992)465.
- [10] A.D. Martin, R.G. Roberts and W.J. Stirling, *Phys. Rev.* **D50**(1994)6734.
- [11] A.D. Martin, R.G. Roberts and W.J. Stirling, preprint RAL-95-021, DTP/95/14,  
hep-ph/9502336.
- [12] C. Peterson, D. Schlatter, I. Schmitt and P. Zerwas, *Phys. Rev.* **D27**(1983)105.
- [13] J. Chrín, *Z. Phys.* **C36**(1987)163.
- [14] S. Frixione, M.L. Mangano, P. Nason and G. Ridolfi, *Nucl. Phys.* **B431**(1994)453.
- [15] A.D. Martin, R.G. Roberts and W.J. Stirling, *Phys. Lett.* **B306**(1993)145,  
*Phys. Lett.* **B309**(1993)492.

- [16] H.L. Lai *et al.*, preprint MSU-HEP-41024, CTEQ-404, hep-ph/9410404.
- [17] A. Vogt, preprint DESY 95-068, hep-ph/9504285.
- [18] H. Abramowicz, K. Charchula and A. Levy, *Phys. Lett.* **269B**(1991)458.
- [19] M. Glück, E. Reya and A. Vogt, *Phys. Rev.* **D46**(1992)1973.
- [20] S. Frixione, M.L. Mangano, P. Nason and G. Ridolfi, *Phys. Lett.* **B319**(1993)339.
- [21] J.C. Collins, D.E. Soper and G. Sterman, in *Perturbative Quantum Chromodynamics*, 1989, ed. A.H. Mueller, World Scientific, Singapore, and references therein.
- [22] M. Glück, E. Reya and A. Vogt, *Phys. Rev.* **D45**(1992)3986.
- [23] C.F. Weizsäcker, *Z. Phys.* **88**(1934)612;  
E.J. Williams, *Phys. Rev.* **45**(1934)729.